Scanning Microscopy

Volume 7 | Number 1 Article 13

1-26-1993

Scanning Electron Microscopy of Muscle Myofibrils After High Pressure Freezing and Freeze-Substitution-Staining

M. Malecki
University of Wisconsin-Madison

M. L. Greaser
University of Wisconsin-Madison

Scanning Microscopy, Vol. 7, No. 1, 1993 (Pages 115-128)
Scanning Microscopy International, Chicago (AMF O'Hare), IL 60666 USA

0891-7035/93$5.00+.00

SCANNING ELECTRON MICROSCOPY OF MUSCLE MYOFIBRILS AFTER HIGH PRESSURE FREEZING AND FREEZE-SUBSTITUTION-STAINING

M. Malecki[1]*, M.L. Greaser[2]

[1]Integrated Microscopy Resource, National Institutes of Health Biotechnology Resource and Molecular Biology Laboratories, and [2]Muscle Biology Laboratory, University of Wisconsin-Madison, Madison, WI

(Received for publication December 10, 1992, and in revised form January 26, 1993)

Abstract

A novel approach to study the three dimensional ultrastructure of organelles and cells by means of scanning electron microscopy is described. Muscle myofibrils have been used in the development of the techniques since their structure is well characterized using conventional electron microscopic methods. Myofibrils in rigor buffer (with no cryo-protectants or pressure sealants) were frozen at high pressure (2300 bar) within specially designed chambers. The frozen specimens were then freeze-substituted-stained with methanol containing tungsten and iron salts and finally critical point dried. These methods allowed scanning electron microscopic observations of the organization of individual filaments within whole myofibrils over several sarcomeres. Images obtained showed excellent structural preservation with three dimensional information which is not available with other electron microscopic techniques. Success in these approaches was ascribed to (**a**) rapid and uniform freezing at high pressure without ice segregation patterns, (**b**) uniform electro-conductivity of the specimen closely attached to the polished carbon piston/carrier, and (**c**) good electron emission (secondary and back-scattered) from the metal incorporated into the myofibril structure without additional coating.

Key Words: Myofibrils, scanning electron microscopy, negative staining, high pressure freezing, freeze substitution, critical point drying, high voltage electron microscopy.

*Address for correspondence:
Marek Malecki
Integrated Microscopy Resource
University of Wisconsin-Madison
1675 Observatory Drive
Madison, WI 53706
Telephone number: 608-263-8481

Introduction

A number of technological difficulties must be overcome to obtain three dimensional images of organelles and cells suitable for structural analysis. It is now clear that chemical fixation to immobilize proteins is too slow compared to the structural reorganization that may occur as a result of ionic fluxes in cells, such as during muscle contraction (Edelman, 1989; Craig *et al.*, 1991). The fastest immobilization method currently available is rapid freezing. Good structural preservation requires vitrification of water. Among a number of available freezing methods, one employing high pressure is particularly suitable because relatively thick specimens may be preserved in a well defined environment until just before cryoimmobilization (Merryman, 1966; Moor and Riehle, 1968; Moor and Hoechli, 1970; Riehle and Hoechli, 1973; Müller and Moor, 1984; Gilkey and Staehelin, 1986; Craig *et al.*, 1987; Studer *et al.*, 1989; McDonald and Morphew, 1989; Dahl and Staehelin, 1989; Malecki, 1990; Malecki and Walther, 1991; Malecki *et al.*, 1991).

Four major methods of processing cryo-immobilized sample for EM imaging have been used following rapid freezing: (**a**) freeze-substitution associated with osmium and uranium fixation-staining followed by embedding and sectioning (Van Harreveld and Crowell, 1964; Pscheid *et al.*, 1981; Humbel and Müller, 1986; Edelman 1989; McDonald and Morphew, 1989; Craig *et al.*, 1991; Craig *et al.*, 1992); (**b**) freeze-fracture followed by etching and surface replication (Heuser and Cooke, 1983; Moor *et al.*, 1980; Gilkey and Staehelin, 1986; Studer *et al.*, 1989); (**c**) freeze-drying followed by metal deposition coating (Gross *et al.*, 1984; Gross, 1987; Hermann and Muller, 1991; Wepf *et al.*, 1992); and (**d**) cryoultramicrotomy (Dubochet *et al*,. 1987; McDowall *et al.*, 1984; Edelman, 1984). These methods, although providing opportunities for high resolution work, yield limited three-dimensional information. In particular we were interested in imaging the three dimensional relationship between the thick, thin, titin-containing, and nebulin-containing filaments in both mature myofibrils and during their assembly. This led us to consider scanning electron microscopy (SEM) and high voltage electron microscopy (HVEM) as imaging tools.

We were particularly encouraged with the results obtained by high pressure frozen specimen preparation for SEM (Malecki, 1990; Malecki and Walther, 1991; Malecki *et al.*, 1991). High resolution SEM work on specimens coated with metal is effective if this metal is thin, continuous and free of structural detail at the magnifications used. In practice, there are numerous problems associated with decoration and radiation damage during metal deposition procedures. These procedures have involved two conventional methods for rendering surfaces electro-conductive. First, deposition of metals with the specimen surface at ambient or low temperatures, results in the presence of coats ranging from 4-6 nm in thickness (Peters, 1980, 1986; Gross *et al.*, 1984; Gross, 1987; Hermann and Müller, 1991). Additionally, this approach is frequently linked to artifactual decoration and radiation damage (Franks *et al.*, 1974; Peters, 1986; Gross *et al.*, 1984). Second, surface binding of several layers of osmium through ligands, results in even thicker coats of 10-14 nm (Kelley *et al.*, 1973; Ip and Fischman, 1979; Murakami and Jones, 1980). This method is frequently associated with severe specimen maceration (Small, 1981; Tanaka, 1981; Tanaka *et al.*, 1991). Both approaches prevented us from clearly observing high resolution ultrastructure within whole myofibrils.

Driven by these observations, we attempted to enhance imaging qualities of myofibrils by employing high pressure freezing in rigor buffer followed by freeze-substitution with concurrent incorporation of metals into the biological structure. In addition, use of a conductive carbon carrier, having atomic mass lower then that of the incorporated metal, was essential for obtaining high resolution images. Initial results on myofibril ultrastructure are described and compared to results obtained with other more conservative approaches.

Materials and Methods

Myofibrils

Myofibrils were prepared from rabbit psoas muscle using the procedures described in Wang and Greaser (1985) as modified by Swartz and coworkers (1990). Myofibrils were stored in 50% v/v (volume/volume) glycerol in rigor buffer [75 mM KCl - 10 mM imidazole (pH 7.2) - 2 mM $MgCl_2$ - 2 mM EGTA - 1 mM DTT] at -20°C. Immediately prior to use, the myofibrils were diluted with 10 volumes of rigor buffer plus 0.1 mg/ml bovine serum albumin (BSA) and pelleted for 10 seconds in a Microfuge. The pellet was resuspended in fresh rigor buffer-BSA and the centrifugation repeated. The final pellet was resuspended in rigor buffer-BSA and held on ice until use (1-2 days).

High pressure freezing

The details of our cryoimmobilization procedures have been described previously (Malecki, 1990) and are only briefly presented here. Spectrographic grade carbon rods [Ted Pella] were sliced and polished before insertion into Teflon [DuPont] cylinders to create specimen wells (Fig. 1). Myofibrils were injected into these wells and immediately tightly covered with gold caps. The closed chambers were then inserted into the high pressure freezer specimen holders (Fig. 2) and located in the specimen chamber of the high pressure freezer [HPM010, Balzers]. Pressure increased to 2300 bar within 10 ms while temperature decreased to -50°C. Carbon rods and gold caps served as pistons, sliding within Teflon cylinders, during this hyperbaric phase of freezing. This action secured effective pressure transfer from the HPM chamber onto the specimen. As the pressure stabilized, the temperature fell to -100°C within the next 10 ms and rapidly dropped to -196°C. The frozen samples were then transferred and stored in liquid nitrogen before further processing.

Freeze-substitution-staining

Frozen myofibrils were transferred from liquid nitrogen into methanol (containing 3% phosphotungstic acid and 3% potassium ferricyanide) that had been precooled to -90°C in the freeze substitution device [FSD 010, Balzers]. Temperatures were maintained at -90°C, -35°C, and 0°C for either 48 hour or 8 hour periods each.

Negative staining

Surfaces of Formvar film/carbon coated grids were rendered hydrophilic by glow discharge [Med 010-Balzers] before use. Myofibrils attached to these grids were negatively stained with either 2% uranyl acetate or 1% ammonium molybdate for 5 minutes before removal of excess stain (Hanson, 1971).

Positive staining

A drop of the myofibril suspension was placed on a Formvar-carbon coated grid and fixed for 1 hour in 2% glutaraldehyde-rigor buffer. After washing in rigor buffer, the grids were inverted over 1% OsO_4 for 10 minutes, washed, inverted over 2% uranyl acetate for 10 minutes, and finally washed. Samples were then critical point dried.

Critical point drying

Specimens in alcohol were transferred into the critical point dryer chamber [Tousimis Samdri] and then dried from the critical point of carbon dioxide (Anderson, 1951; Ris, 1985).

Electron microscopy

Myofibril whole mounts were observed in the Hitachi S900 SEM operated at 1-30 kV in the secondary electron emission (SE) mode or at 2.7-30 kV in the backscattered electron (BSE) mode. The microscope was equipped with the Gatan cryostage, a cold blade immediately adjacent to the specimen, and the original Hitachi cryotrap. Specimen carriers, serving formerly also as pistons during hyperbaric freezing, were assembled into the cryostage with a specially designed cryoholder (Figs. 3 and 4).

Alternatively, samples were viewed in the Associated Electric Industries (AEI) High Voltage Electron

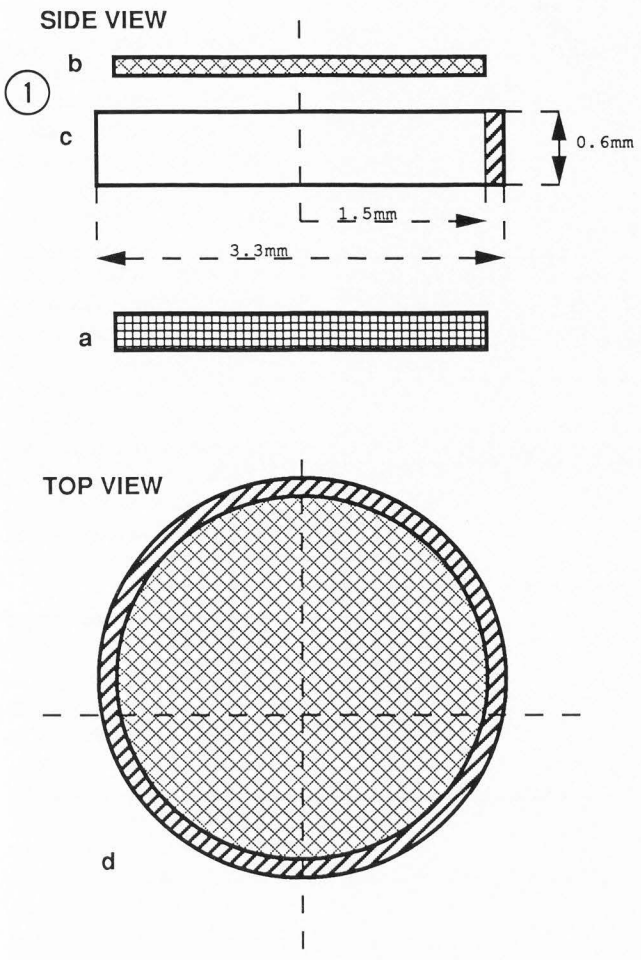

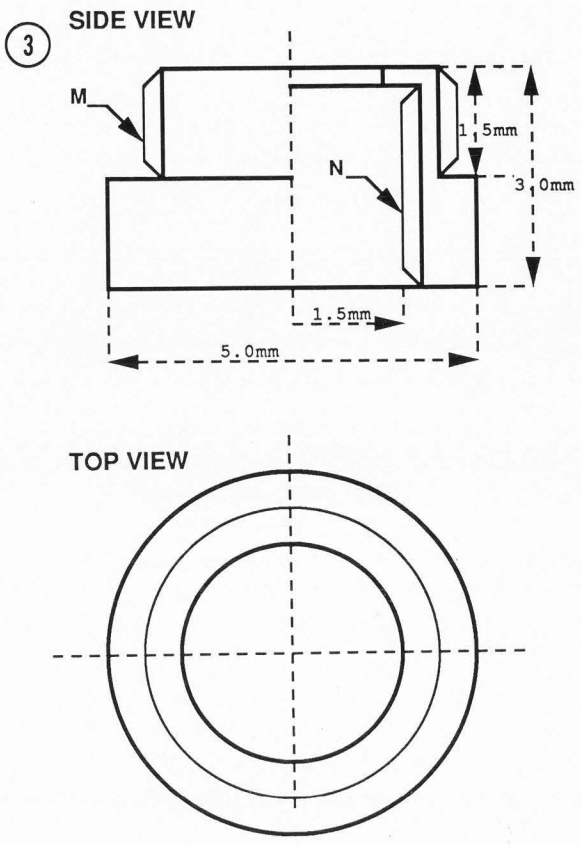

Figure 1. Diagram of the specimen chamber for high pressure freezing. (**a**) polished carbon piston, (**b**) gold piston, (**c**) Teflon or copper cylinder, (**d**) chamber assembled.

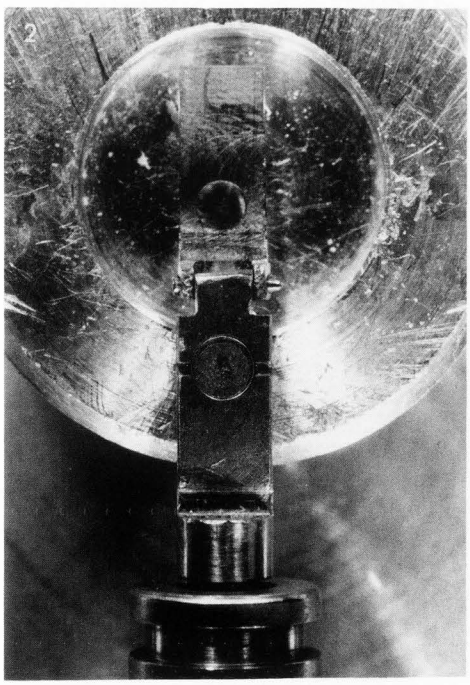

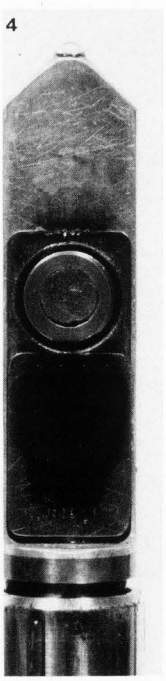

Figure 2. Photograph of the specimen chamber described in Figure 1 assembled into a freezing holder tip of the High Pressure Freezer [HPM 010, Balzers].

Figure 3. Diagrams of the specimen cryo-holder accepting specimens carriers from high pressure freezing. M: External thread for transfer tools; N: internal thread for locking screw.

Figure 4. Photograph of the specimen holder described in Figure 3 assembled into the Gatan cryostage tip.

Microscope, Mark 7 Type II. The microscope was operated at 1 MeV accelerating voltage. The microscope stage had rotating-tilting capability.

Results

Myofibrils were high pressure frozen, freeze-substituted-stained, and critical point dried. These myofibrils remained attached to the polished carbon carriers, that had previously served as pistons during hyperbaric freezing. The samples were observed on the Gatan cryostage at -100°C in the Hitachi S900 (Fig. 5-9). These

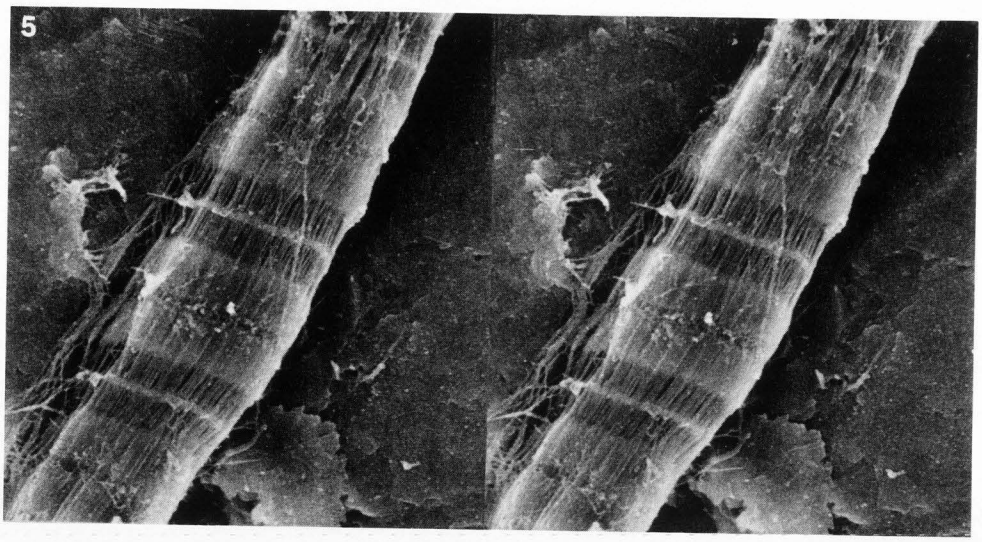

Figure 5. Stereo-image of a myofibril on a polished carbon carrier (serving formerly during hyperbaric freezing as a piston) after high pressure freezing, freeze-substitution-staining, and critical point drying. The myofibril ultrastructure is well preserved over several sarcomeres. Bands and Z lines are clearly organized. SE mode; accelerating voltage (AV) = 15 kV; horizontal field width (HFW) = 5.85 μm.

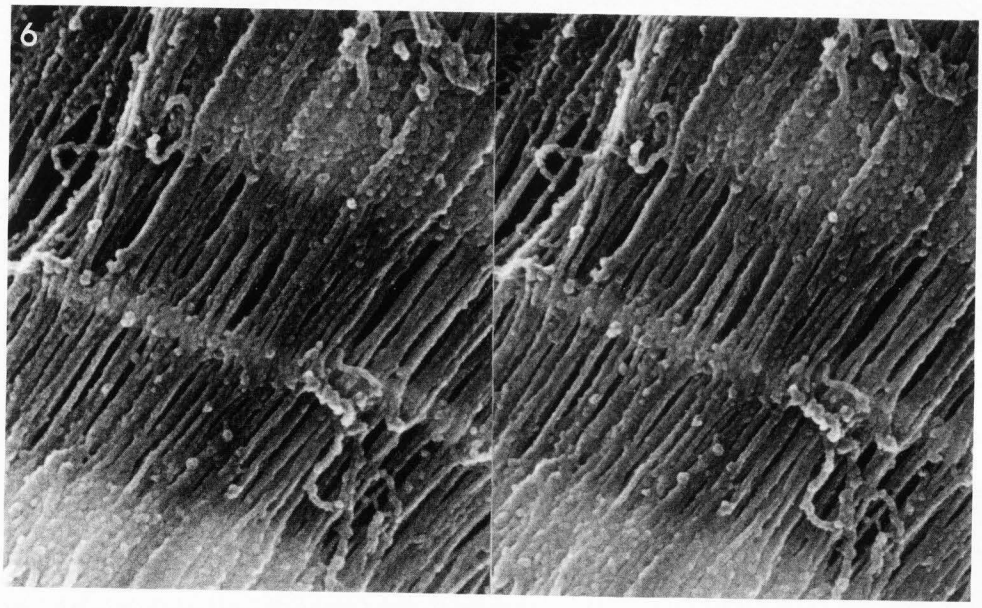

Figure 6. Stereo-image of a selected region of the same myofibril as in Fig. 5 (near the bottom Z line). Individual filaments are easily recognized and the three-dimensional organization of the filament interactions can be appreciated. SE mode; AV = 15 kV; HFW = 1.3 μm.

myofibrils had band distributions similar to those observed previously using other microscope techniques. No ice segregation patterns were present. The procedures used avoided the three most common problems associated with specimen freezing. First, the myofibrils were frozen in a salt containing buffer but not cryoprotected, washed with water, or treated with chamber sealing agents. Second, these myofibrils were maintained within closed chambers which protected them from drying. Due to these two features, potential artifacts encountered before freezing due to osmolality or ionic strength changes (which can result in lattice spacing, protein extraction, or filament depolymerization) were avoided. Third, the design of the chamber allowed effective pressure transfer and high freezing rate. It was demonstrated by recent studies that freezing rate during hyperbaric cryoimmobilization is sufficiently high to prevent ionic shifts (Zierold *et al.*, 1991). Furthermore X-ray diffraction studies have shown that freeze-substitution preserves molecular organization below 3 nm resolution (Erk *et al.*, 1991). Thus the images obtained by our new procedure represent snapshot views of structures reasonably close to that found in the living state.

Myofibrils had well defined band patterns over several sarcomeres. A bands, I bands, and Z lines were clearly distinguished (Fig. 5). Image detail was significantly enriched by working at higher magnifications. The sarcomere three-dimensional organization could be appreciated in stereopairs (Figs. 6-8). Individual thick and thin filaments were clearly distinguished. As

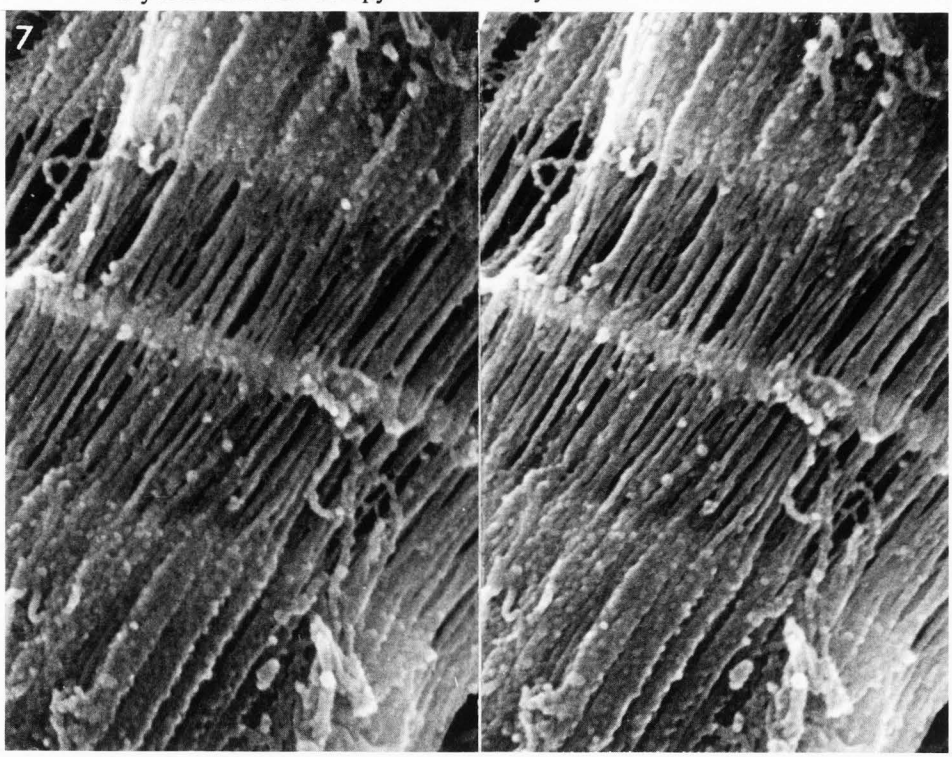

Figure 7. The same region as in Fig. 6, but recorded at reduced accelerating voltage. Images of individual filaments were less distinct. SE mode; AV = 5 kV; HFW = 1.3 μm.

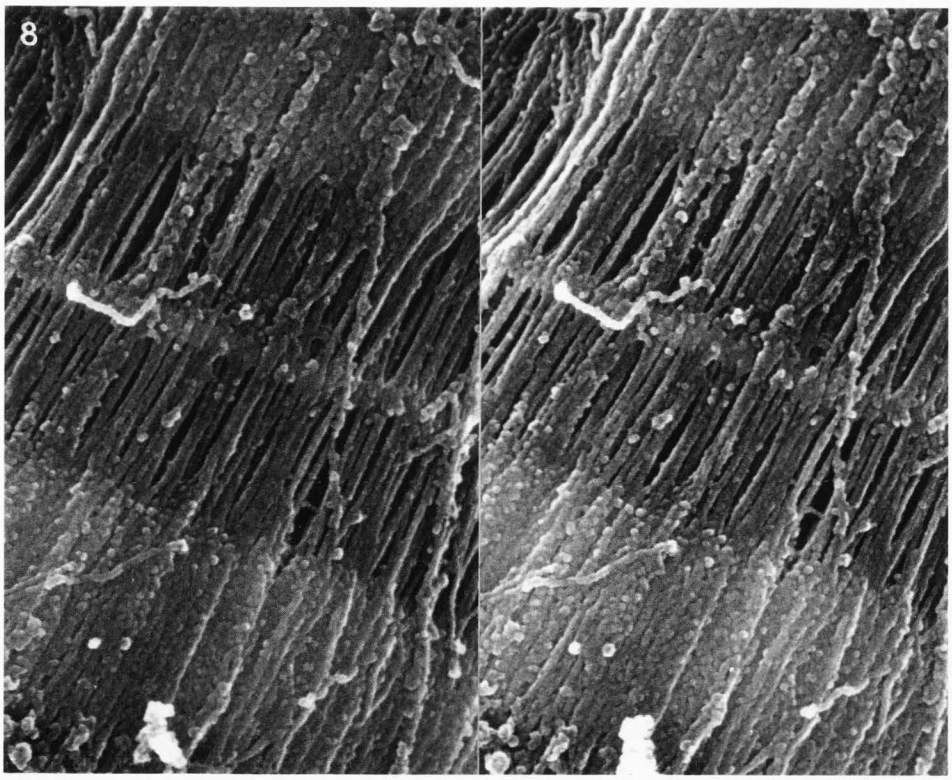

Figure 8. The same myofibril as in Fig. 5 (region shown is near the second Z line from the top), but recorded at the higher voltage. The fine structure on the surface of the individual filaments is visible. SE mode; AV = 25 kV; HFW = 1.3 μm.

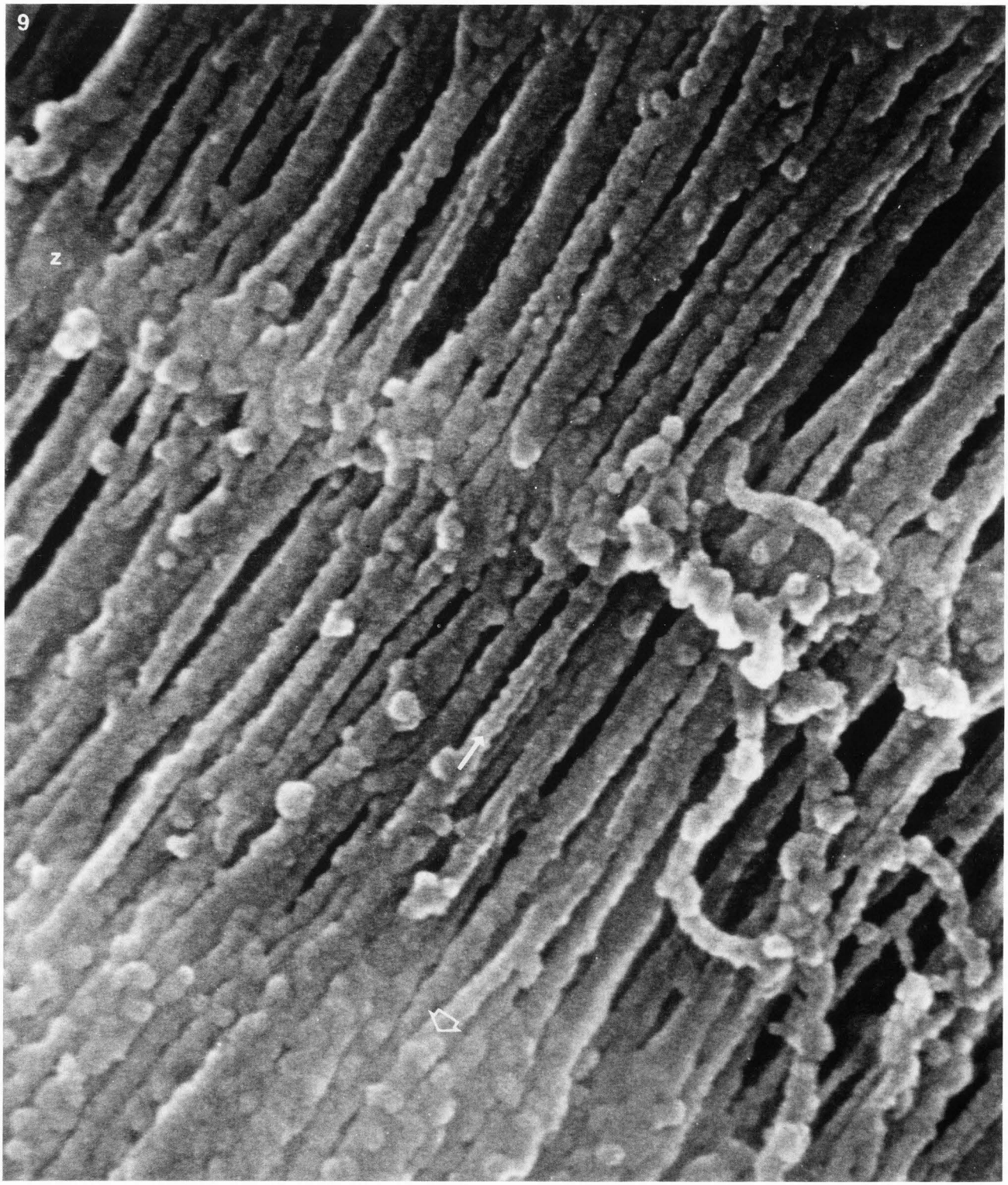

Figure 9. High magnification view of the same myofibril as in Figs. 5-8. The area shown is from the region near the Z line in Fig. 8. Surface features on the thin filaments are visible (thin arrow). Note the bulb-like structures on the thick filaments that presumably represent the myosin heads (wide arrow). SE mode; AV = 25 kV; HFW = 288 nm.

expected, striking differences were noted in image quality when different accelerating voltages were used. At low voltages mostly surface features were revealed due to reduced electron penetration; however, contrast was also enhanced (Fig. 7). Higher voltages resulted in recognition of finer ultrastructural details. However, greater contributions from deeper regions of the specimen were also noticed (Fig. 6). The ultrastructure of individual 6 nm filaments was more detailed at high (Fig. 8) than at low voltage (Fig. 7). Surface irregularities within these filaments may correspond to the actin monomers (Fig. 9, arrow), but the subunit arrangement was partially obscured by the tropomyosin/troponin/nebulin in the helical grooves compared to images obtained previously with purified F-actin filaments (Wepf *et al.*, 1992). Thick filaments had clearly identifiable central bare zones. Globular structures were visible on the distal portions of the thick filaments that presumably represent the myosin heads (Fig. 9, large arrow). Patterns observed previously using negative staining of isolated thick filaments or sections of freeze-substituted muscle have required image enhancement to see the individual myosin heads.

In specimens covered with evaporated metal, suitable imaging conditions would be expected over the entire conductive specimen only as long as the thin metal layer was continuous and uniformly distributed. This is difficult to achieve in practice. In contrast, specimens impregnated with metal according to our protocols had uniform electrical properties across the whole myofibril, so the images were more sensitive to voltage variability depending on the structure's compactness. As a consequence, thin filaments having small diameters had reduced electron extraction volumes (Joy *et al.*, 1982; Pawley *et al.*, 1991). In the densely packed areas and at the high voltages, emission from the structures deep underneath contributed to final signals from the surface (Fig. 8). Study of these areas was possible using reduced accelerating voltages to limit the depth of beam penetration and electron extraction, but this was a compromise at the expense of resolution (Fig. 7). However, higher voltage along with samples having good electroconductivity yielded more detailed images (Fig. 9). This might be explained on the basis of earlier reports that higher voltages resulted in a smaller spot size (Nagatani and Saito, 1986), and induced electro-conductivity (Leamy *et al.*, 1978; Jakubowicz, 1987) and ability to overcome local electrostatic fields by highly energetic electrons (Peters, 1986). Nevertheless, in all cases, the use of the cryostage cold-trap and adjacent cold blades was essential to prevent rapid contamination.

Effectiveness of metal incorporation was evaluated by imaging in the backscattered electron (BSE) mode. Images were obtained using the main cold trap only, since the inserted BSE detector excluded simultaneous usage of the adjacent cold blade. In this mode, myofibrils with incorporated metal were quickly recognized as very bright spots over a dark background (Fig. 10). The metal incorporation was observed even after the short protocol of freeze-substitution-staining. Electrons were backscattered efficiently only from myofibrils. In contrast, samples that had been sputter coated had metal coats covering the myofibrils as well as the support carriers. Also, we did not pursue studies employing methods similar to those applied for preparing platinum-carbon replicas (carbon stabilization of metal stained samples), since the necessary carbon coating would obscure fine ultrastructural details in the SE mode. Finding myofibrils was more difficult in the SE mode and at low voltages (Fig. 11). Work at low voltages would allow observations even on untreated, weakly conducting specimens, and comparison of images in both modes. Thus, myofibril structure was recognized in both modes based on topographical contrast (SE) and atomic mass content (BSE). General myofibril organization was easily recognized (A bands, I bands, Z lines) at higher magnification and in BSE mode (Fig. 12). The distribution and uniformity of metal incorporation could be observed. The same myofibril could then be imaged in the SE mode (Fig. 13). Individual 5 nm gold beads introduced into the specimen before freezing were clearly visible. Sufficient metal incorporation to detect individual filaments occurred even after the short freeze substitution staining procedure. In both cases, carbon carriers played a crucial role in providing good electro-conductivity. Attempts to apply similar protocols with myofibrils attached to glass were never as successful as those with polished carbon. These myofibrils had been partially extracted with sodium pyrophosphate before processing (Figs. 10-13). Additional studies using various methods to expand the compact myofibril structure are in progress.

The methods we have developed for studying myofibril whole mounts were compared to other preparation and imaging techniques, namely, HVEM after negative staining or after positive staining and critical point drying. HVEM offered enhanced beam penetration, improved resolution, and reduced specimen damage at high accelerating voltage compared to normal TEM (Glaeser, 1974). Indeed, negatively stained samples provided images of paracrystalline arrays of thick filaments (Figs. 14 and 15). In these samples, the periodicity due to the C protein stripes and the myosin cross-bridges (perpendicular lines distal to the C protein zones) can be readily recognized. Periodicity (38 nm) due to the troponin complex in the I band was also visible. The observed images were two-dimensional projections of many filament layers from the myofibril. This resulted in very complex images with structural overlap. Overlap of periodic structures provides information about repeats; however, direct observation of individual filaments in the context of a whole myofibril was very difficult. Furthermore, when alignment of filaments was not optimal with regard to the electron axis, structural interpretation became difficult. Myofibrils were also observed in the HVEM after fixation, staining, and critical point drying. At low magnifications (Fig. 16), individual sarcomeres, A bands, I bands, and Z lines could


10

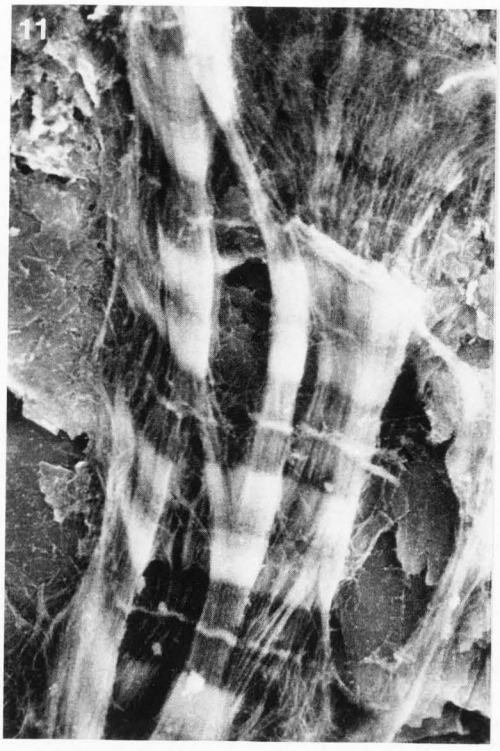
11

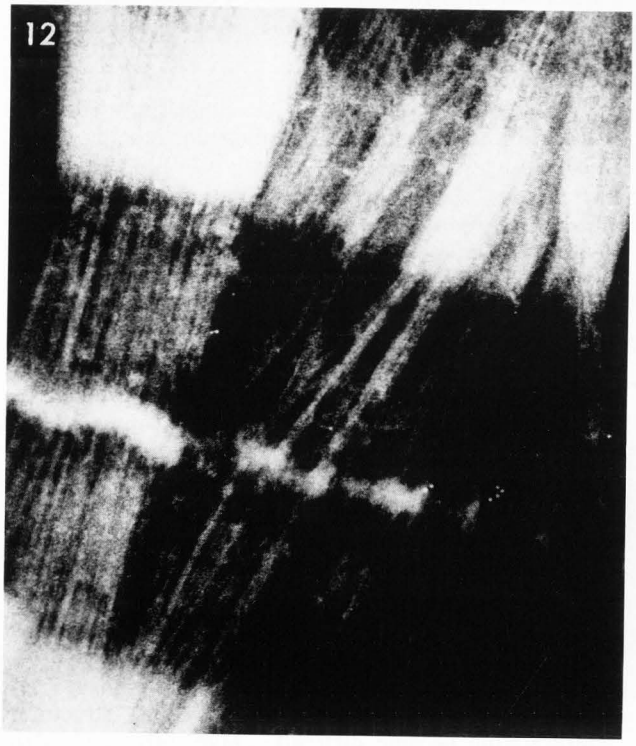
12

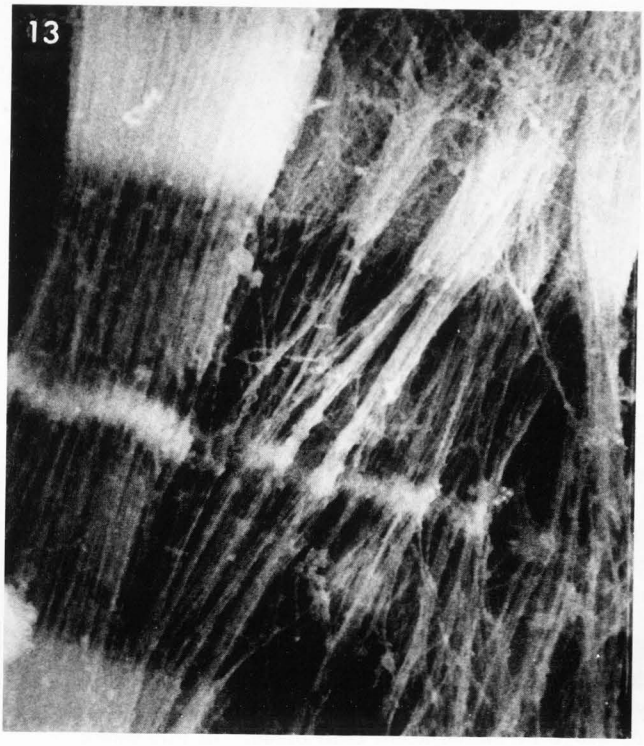
13

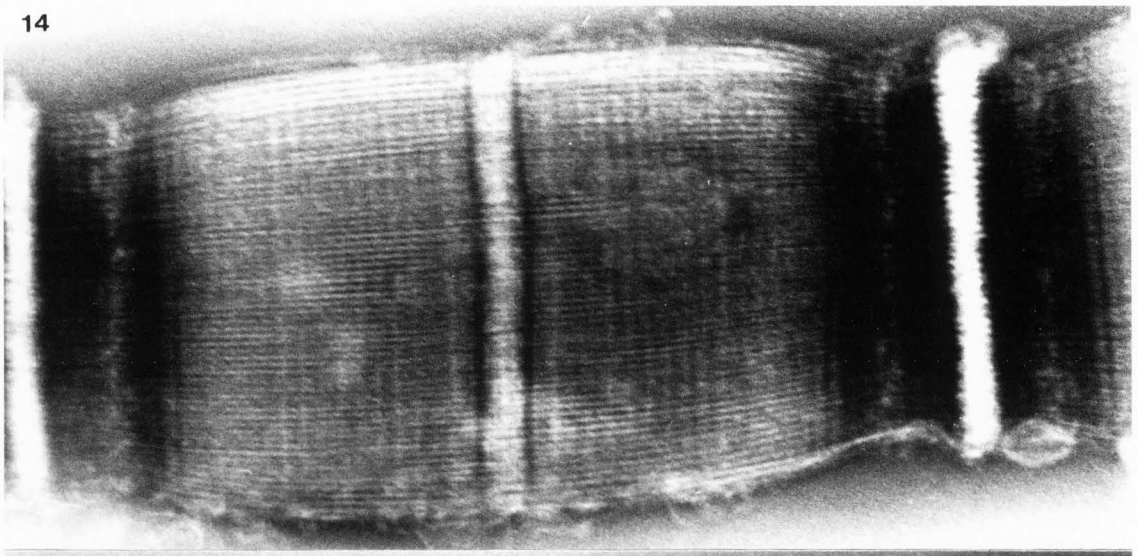

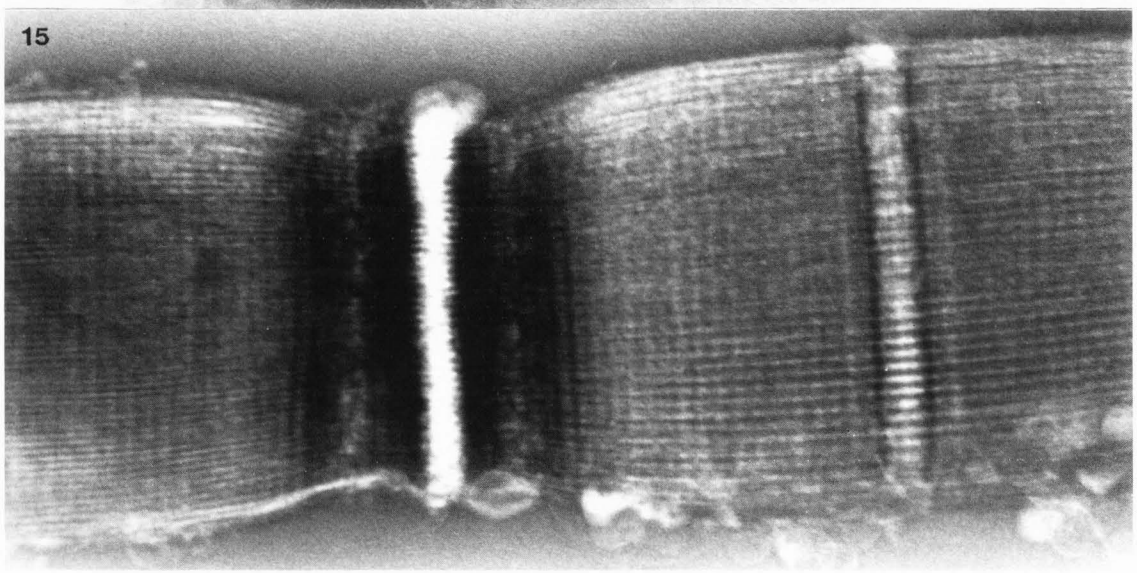

Figure 10. Myofibril image after high pressure freezing, freeze-substitution-staining (short protocol), and critical point drying. Myofibrils were partially swollen in sodium pyrophosphate before freezing. The large difference in atomic mass between tungsten and the carbon support gave very high contrast and facilitated localization of the myofibrils. BSE mode; AV = 7 kV; HFW = 5.85 μm.

Figure 11. The same myofibrils as in Fig. 10, but in the SE mode. Myofibrils were harder to find at low voltages, but contrast within the structure was good. SE mode; AV = 1.5 kV; HFW = 5.85 μm.

Figure 12. A higher magnification view of the myofibrils in Fig. 10 (region near the center Z line). Individual filaments are easily recognized due to incorporated metal. The bright spots are gold beads (5 nm) introduced before freezing as a metal incorporation and size reference. BSE mode; AV = 7 kV; HFW = 1.3 μm.

Figure 13. A higher magnification view of the myofibrils in Fig. 11 (region near the center Z line). The surface topography of the filaments can be observed without any further metal coating. SE mode; AV = 1.5 kV; HFW = 1.3 μm.

Figure 14. Myofibrils negatively stained with 2% uranyl acetate and imaged in the HVEM. Note that projections of the superimposed thick filaments showed the periodicity ascribed to C protein and the myosin cross bridges. AV = 1 MeV; HFW = 2.7 μm.

Figure 15. A different part of the same myofibril as in Fig. 14. Note that the hexagonal thick filament lattice in the A band appears different in the half A bands on opposite sides of the Z line. AV = 1 MeV; HFW = 2.7 μm.

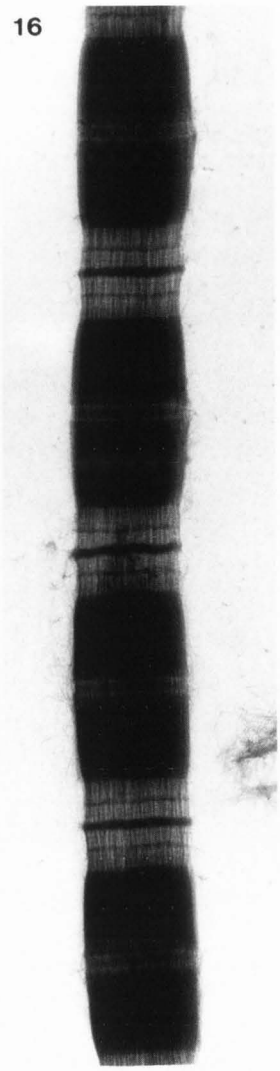

Figure 16. Whole mount myofibrils after positive staining with uranyl acetate and critical point drying imaged in HVEM. The metal staining provided adequate contrast to clearly distinguish the banding pattern and Z lines. AV = 1 MeV; HFW = 2.56 μm.

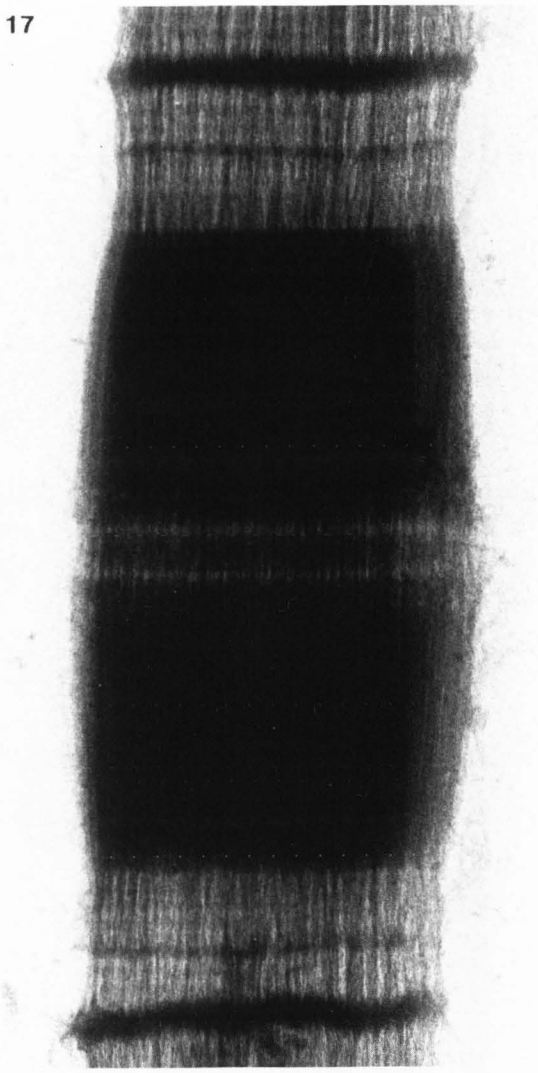

Figure 17. Same whole mount myofibril as shown in Fig. 16 at a higher magnification. The overlap of many filaments in one projection plane obscured most of the fine structure. AV = 1 MeV; HFW = 1.52 μm.

be clearly recognized. At high magnifications (Fig. 17), some individual filaments were visible, but these could only be identified if they were partially detached or very near the lateral edges (overlap of filament images from multiple levels in the Z axis obscured the individual filament ultrastructure).

Discussion

Our major concern throughout this project was to develop techniques to analyze the three dimensional organization of organelles and cells using whole myofibrils as a test specimen. There were three factors contributing to the success of the current approach. First, myofibrils were maintained in salt containing buffers (more like their natural environment) until just before cryoimmobilization. Furthermore, the new design of a specimen holder for high pressure freezing ensured effective pressure transfer and resulted in uniform freezing without ice segregation patterns. Second, problems with specimen charging in the SEM were eliminated by making samples uniformly conductive across their entire thickness and by using polished carbon pistons as sample carriers. Third, secondary or backscattered electron emission from metal incorporated into the samples during freeze-substitution-staining provided sufficient signal for the detectors without additional metal coats that might obscure the fine ultrastructure.

A comparison of the current approach to methods used previously is illustrated in Fig. 18. Negative staining of native structures provides sharp outlines of biological structures. The use of HVEM with its greater beam penetration allows observation of thicker specimens, but interference from structures at different depths makes structural interpretation difficult. Thus,

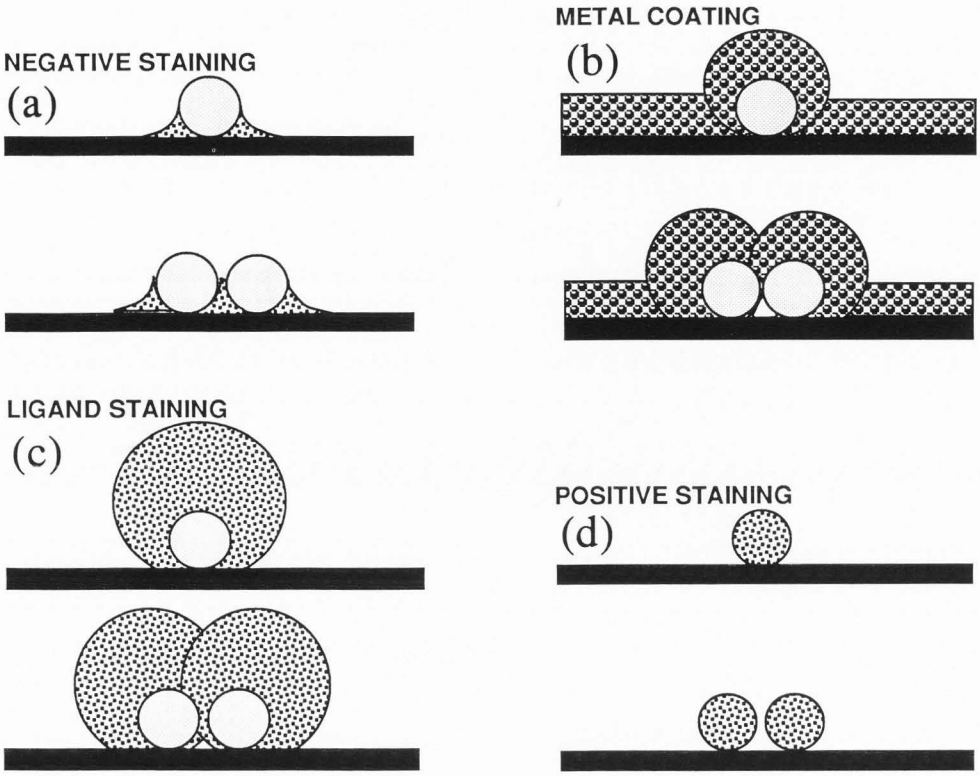

Figure 18. Diagrams showing the effects of different specimen preparation techniques on image resolution. **(a)** Negative staining. The differences in electron scattering between the specimen and the surrounding heavy metal provide high resolution images with TEM or HVEM. **(b)** Metal coating. Non-conductive specimens must be covered with 6 nm of metal (depending on the metal and deposition method) to ensure adequate conductivity and secondary emission. Thus, adjacent filaments or structures in this size range will not be resolved. **(c)** Ligand staining (osmium-tannic acid-osmium procedure). Improved conductivity on the structure surface is provided from several layers of metal absorbed on top of each other through ligand bonds. **(d)** Positive staining. Metal is directly incorporated into the structure or as a very thin layer on its surface, allowing excellent spatial resolution. This type of staining occurs in the new freeze-substitution-staining method described here.

---

this approach is limited to specimens having paracrystalline arrangement or specimens observed using stereo-imaging systems (Malecki, 1990). Transmission electron microscopy is the observation method available for negatively stained materials. Observation of samples in the SEM requires sufficient conductivity to prevent charging and enough electron emission (secondary or backscattered) to obtain a good signal. This is usually accomplished by coating of the weakly conductive specimens with metal. The evaporated metal coat (Fig. 18) must be thin, continuous, and free of its own substructure. A metal layer of 4-6 nm is typically required to obtain an adequate signal (Gross *et al.*, 1984; Gross, 1987; Peters, 1980, 1986; Hermann and Müller, 1991). Such a thick metal coat will obscure structural details and surface features on objects less than 10 nm in diameter. Structures separated by less than a double thickness of the metal coat are then impossible to resolve. Moreover, existing procedures have been developed and applied only to very thin specimens (Hermann and Müller, 1991; Wepf *et al.*, 1992); they prove to be inadequate for thicker biological specimens like myofibrils or fractured cells. Since the electro-conductivity was only associated with the superficial layer, any coating discontinuity or break will result in immediate charging and resolution deterioration. A third approach (Fig. 18) uses several layers of osmium linked to the specimen through ligands (Kelley *et al.*, 1973; Ip and Fischman, 1979; Murakami and Jones, 1980). Penetration of osmium improved overall conductivity of the specimen, but also introduced an extra coating of 10-14 nm over the structures, and therefore, diminished resolution. Thus, in this approach, the charging problem can be potentially overcome, but only at the expense of resolution. A fourth approach (Fig. 18) uses metal incorporated into structures as a part of chemical fixation and staining protocols at ambient temperatures to ensure adequate contrast for TEM. This has also been done during freeze-substitution with media containing osmium and uranium followed by embedding and ultramicrotomy

(Van Harreveld and Crowell, 1964; Pscheid *et al.*, 1981; Humbel and Müller, 1986; Craig *et al.*, 1992) or followed by critical point or freeze-drying for TEM (Bridgman and Reese, 1984). Attempts to stain samples along with conventional surface coating techniques for SEM, although providing enhanced imaging qualities for whole cell studies, appeared to be insufficient for high resolution observation (Malecki and Walther, 1991).

In our approach, whole mount frozen samples were exposed to metal ions in the freeze-substitution media at very low temperatures (Fig. 18). Samples were maintained in the cold from freezing through observation. This approach gave minimal change in filament diameters or spacing and very high resolution images with three dimensional information. In addition to further studies on myofibril and filament ultrastructure that are in progress, this method should have wide application to imaging structures near the limit of microscopic resolution.

Acknowledgments

This work was supported by the College of Agricultural and Life Sciences, University of Wisconsin-Madison and grants from USDA (91-37206-6743) and NIH (DRR-570). We wish to thank Nina Malecki and Eric Landmark for assistance with photography and drawings. We also thank Bob Sandberg for access to the College of Engineering Workshops and Mr. Ray Schendel for help in manufacturing of consecutive designs of cryo-holder and cryo-chamber. Discussions with Drs. Hans Ris, Stan Erlandsen and David Spector are greatly appreciated.

References

Anderson TF (1951) Techniques for the preservation of three dimensional structures in preparing specimens for electron microscopy. Trans NY Acad Sci **13**: II, 130-134.

Bridgman PC, Reese TC (1984) The structure of cytoplasm in directly frozen cultured cells. I. Filamentous networks and cytoplasmic ground substance. J Cell Biol **99**, 1655-1668.

Craig R, Alamo L, Padron R (1992) Structure of the myosin filaments of relaxed and rigor vertebrate striated muscle studied by rapid freezing electron microscopy. J Mol Biol **228**, 474-487.

Craig S, Gilkey JC, Staehelin LA (1987) Improved specimen support cups and auxiliary devices for the Balzers high pressure freezing apparatus. J Microsc **148**, 103-106.

Craig R, Padron R, Alamo L (1991) Direct determination of myosin filament symmetry in scallop striated adductor muscle by rapid freezing and freeze substitution. J Mol Biol **220**, 125-132.

Dahl R, Staehelin LA (1989) High-pressure freezing for the preservation of biological structure: Theory and practice. J Electr Microsc Techn **13**, 165-174.

Dubochet J, Adrian M, Chang JJ, Lepault J, McDowall AW (1987) Cryoelectron microscopy of vitrified specimens. In: Cryotechniques in Biological Electron Microscopy. Steinbrecht RA, Zierold K (eds.), Springer Verlag, 491-501.

Edelman L (1984) Frozen hydrated cryosections of thallium loaded muscle. Physiol Chem and Mol NMR **16**, 499-501.

Edelman L (1989) The contracting muscle: The challenge for freeze-substitution and low temperature embedding, Scanning Microsc Suppl **3**, 241-252.

Erk I, Delacroix H, Nicolas G, Ranck JL, Lepault J (1991) Cryoelectron microscopy of vitrified specimens: an approach to the study of bulk specimens. J Electr Microsc Techn **18**, 406-410.

Franks J, Clay CS, Peace GW (1974) Ion beam thin film deposition. Scanning Electron Microsc **1974**, 155-162.

Gilkey JC, Staehelin LA (1986) Advances in ultrarapid freezing for the preservation of cellular ultrastructure. J Electr Microsc Techn **3**, 177-210.

Glaeser RM (1974) Radiation damage and resolution limitations in biological specimens. In: High Voltage Electron Microscopy. Swann PR, Humphreys CY, Goringe MH (eds.), Academic Press, 370-378.

Gross H (1987) High resolution metal replication of freeze-dried specimens. In: Cryotechniques in Biological Electron Microscopy. Steinbrecht RA, Zierold K (eds.), Springer Verlag, 205-215.

Gross H, Müller T, Wildhaber I, Winkler H, Moor H (1984) Freeze fracture and replication at -260°C. In: Proc Ann Mtg Electron Microsc Soc America. San Francisco Press, 12-15.

Hanson J (1971) Structure of the myosin containing filament assembly (A-segment) separated from frog skeletal muscle. J Mol Biol **58**, 65-87.

Hermann R, Müller M (1991) High resolution biological scanning electron microscopy: A comparative study of low temperature metal coating techniques. J Electr Microsc Techn **18**, 440-449.

Heuser J, Cooke R (1983) Actin-myosin interactions visualized by the quick-freeze, deepetch, replica technique. J Mol Biol **169**, 97-122.

Humbel B, Müller M (1986) Freeze substitution and low temperature embedding. In: The Science of Biological Specimen Preparation for Microscopy and Microanalysis 1985. Müller M, Becker RK, Boyde A, Wolosewick JJ (eds.), Scanning Electron Microscopy, AMF O'Hare (Chicago), IL, 175-183.

Ip W, Fischman DA (1979) High resolution scanning electron microscopy of isolated and in situ cytoskeletal elements. J Cell Biol **83**, 249-254.

Jakubowicz A (1987) Theory of electron beam induced current and cathodoluminescence contrast from structural defects of semiconductor crystals: steady-state and time-resolved. Scanning Microsc **1**, 515-533.

Joy DC, Newbury DE, Myklebust RL (1982) The role of fast secondary electrons in degrading spatial resolution in the analytical electron microscope. J

Microsc **128**, RP1-RP2.

Kelley RO, Dekker RA, Bluemink JG (1973) Ligand-mediated osmium binding: Its application in coating biological specimens for SEM. J Ultrastruct Res **45**, 254-258.

Leamy HJ, Kimerling LC, Ferris SD (1978) Electron beam induced current. Scanning Electron Microsc **1978**; I: 717-726.

Malecki M (1990) High voltage electron microscopy and low voltage scanning electron microscopy of neoplastic cell culture. Scanning Microsc Suppl **5**, S53-S73.

Malecki M, Pawley J, Ris H (1991) High pressure freezing of cells in suspension for LVSEM. In: Proc 49th Ann Mtg Electron Microsc Soc America. San Francisco Press, **3**, 64-65.

Malecki M, Walther P (1991) High pressure freezing of cell aggregates for ultrastructural studies with LVSEM and HVEM. Scanning **13**, 68-69.

McDonald K, Morphew M (1989) Preservation of embryo ultrastructure by high pressure freezing. In: Proc 47th Ann Mtg Electr Microsc Soc America. San Francisco Press, 994-995.

McDowall AW, Hoffman W, Lepault J, Adrian M, Dubochet J (1984) Cryoelectron microscopy of vitrified insect flight muscle. J Mol Biol **178**, 105-111.

Merryman HT (1966) Review of biological freezing. In: Cryobiology. Merryman HT (ed.), Academic Press, 1-114.

Moor H, Bellin G, Sandri C, Akert K (1980) The influence of high pressure freezing on mammalian nerve tissue. Cell Tissue Res **209**, 201-216.

Moor H, Hoechli M (1970) The influence of high pressure freezing on living cells. In: Proc 7th Congr Electron Microsc. Favard P (ed.), Soc Francaise de Microsc Electronique, Paris, **1**, 445-446.

Moor H, Riehle U (1968) Snap freezing under high pressure. In: Proc 4th Eur Reg Conf Electron Microsc. Bonairelli S (ed.), Poliglotta Vaticana, Rome, **2**, 33-34.

Müller M, Moor H (1984) Cryofixation of thick specimens by high pressure freezing. In: The Science of Biological Specimen Preparation for Microscopy and Microanalysis. Revel JP, Barnard T, Haggis GH (eds.), Scanning Electron Microscopy, Chicago, 131-138.

Murakami T, Jones AL (1980) Conductive staining of biological specimens for non-coated scanning microscopy; double staining by tannin osmium and thiocarbohydrazide osmium methods. Scanning Electron Microsc **1980**; I: 221-226.

Nagatani T, Saito S (1986) Instrumentation for ultrahigh resolution scanning electron microscopy. Proc 11th Int Cong Elect Microsc **3**, Jap. Soc. Electron Microscopy, Tokyo, Japan, 2101-2104.

Pawley JB, Walther P, Shih SJ, Malecki M (1991) Early results using high resolution, low voltage, low temperature SEM. J Microscopy **161**, 327-335.

Peters K (1980) Penning sputtering of ultrathin metal films for high resolution electron microscopy. Scanning Electron Microsc **1980**; I, 143-154.

Peters KR (1986) Metal deposition by high energy sputtering for high magnification electron microscopy. In: Advanced Techniques in Biological Electron Microscopy. Koehler JK (ed.), Springer Verlag, 101-166.

Pscheid P, Schmidt C, Plattner, H (1981) Cryofixation of monolayer cell cultures for freeze-substitution. J Microscopy **121**, 149-167.

Riehle U, Hoechli M (1973) The theory and technique of high pressure freezing. In: Freeze Etching: Techniques and Applications. Benedetti EL, Favard P (eds.), Soc Francaise de Microsc Electronique, Paris, 31-61.

Ris H (1985) The cytoplasmic filament system in critical point dried whole-mounts and plastic-embedded sections. J Cell Biol **100**, 1474-1487.

Small JV (1981) Organization of actin in the leading edge of cultured cells: effects of osmium and dehydration on the ultrastructure of actin meshworks. J Cell Biol **91**, 698-705.

Studer D, Michel M, Müller M (1989) High pressure freezing comes of age. Scanning Microsc Suppl **3**, 253-269.

Swartz, DR, Greaser ML, Marsh BB (1990) Demonstration of the steric-blocking mechanism in isolated rigor myofibrils using fluorescent sub-fragment 1. J Cell Biol **111**, 2989-3001.

Tanaka K (1981) Demonstration of intracellular structures by high resolution SEM. Scanning Electron Microsc **1981**; II, 1-8.

Tanaka K, Mitsushima A, Yamagata N, Kashima Y, Takayama H, (1991) Direct visualization of colloidal gold bound molecules and cell-surface receptor by ultrahigh resolution SEM. J Microscopy **161**, 455-461.

Van Harreveld A, Crowell J (1964) Electron microscopy after rapid freezing on a metal surface and substitution fixation. Anat Rec **149**, 381-386.

Wang S-M, Greaser ML (1985) Immuno-cytochemical studies using a monoclonal antibody to bovine cardiac titin on intact and extracted myofibrils. J Muscle Res Cell Motil **6**, 293-312.

Wepf R, Bremer A, Amrein M, Aebi U, Gross H (1992) Surface imaging of F actin filaments; a comparative study by SEM, TEM and STM. Electron Microsc **3**, Secr. Publ. Univ. Granada, Spain, 751-753.

Zierold K, Michel M, Müller M (1991) X-ray analysis of high pressure frozen and impact frozen erythrocytes. J Microsc **161**, RP1-RP2.

Discussion with Reviewers

Reviewer I: The higher magnification images (e.g., Fig. 7) seem to show a "step" at the end of the A-band, with several layers of thick filaments apparently ending "in space". Have layers of thin filaments been etched away at some stage of preparation?

Authors: We do not believe any filaments have been etched away. The lack of thin filaments on the surface of the myofibril may be more apparent than real. The

irregular surface bumps on the thick filaments are more visually prominent.

Reviewer I: Do relaxed myofibrils look better or worse preserved than rigor myofibrils, and are individual thick filaments more readily seen when the cross-bridges are not attached to the thin filaments?
Authors: Relaxed and rigor myofibrils have not been compared so far but these experiments are planned. Such experiments are very difficult with existing methods.

Reviewer I: Can the authors see ways of examining activated myofibrils by these methods?
Authors: Yes. All that is required is the rapid mixing of myofibrils with a buffered, physiological ionic strength, ATP-magnesium-calcium mixture immediately before freezing.